water

MDPI

Article

Evolution of Hydrodynamic Characteristics with Scour Hole Developing around a Pile Group

Yilin Yang [1], Meilan Qi [1,*], Jinzhao Li [2] and Xiaodong Ma [1]

[1] School of Civil Engineering, Beijing Jiaotong University, Beijing 100044, China; yilinyang@bjtu.edu.cn (Y.Y.); 17121074@bjtu.edu.cn (X.M.)

[2] National Engineering Laboratory of Port Hydraulic Construction Technology, Tianjin Research Institute of Water Transport Engineering, Tianjin 300456, China; kingle@bjtu.edu.cn

* Correspondence: mlqi@bjtu.edu.cn; Tel.: +86-010-5168-4390

Received: 14 October 2018; Accepted: 8 November 2018; Published: 12 November 2018

Abstract: This study concerns the evolution of flow field and hydrodynamic characteristics within the developing scour hole around a four-pile group with 2 × 2 arrangement. The instantaneous velocities in scour holes at four typical stages during the scouring process were measured by an acoustic Doppler velocimeter (ADV). The evolution and spatial distribution of the time-averaged flow field, turbulence, and the corresponding hydrodynamic characteristics within scour holes were compared. The time-averaged flow field shows that the reverse flow, downward flow, and horseshoe vortex are formed in the upstream of the pile group. During the scouring process, the mean components of flow characteristics (i.e., mean velocity, vorticity, and bed shear stress) around the pile group decrease while the fluctuating components (i.e., turbulence intensity) intensify simultaneously. Similarity of turbulence intensity profiles was found within different scour holes. The horseshoe vortex at upstream of each pile merges and the shear layer in the gap region extends when the dimension of the scour hole increases to that of equilibrium scour status, indicating that the four piles behave more like a single bluff body. With the development of scour holes, the large-scale horseshoe vortex system becomes more stable and the dissipation of small-scale eddies becomes more significant.

Keywords: scour hole; horseshoe vortex; pile group; flow field; turbulence intensity; energy spectra analysis

1. Introduction

Pile-group foundations are widely used in practice to support structures [1], such as bridges, offshore oil platforms, offshore wind power equipment, etc. The presence of a pile group changes the local flow field, and the strengthened hydrodynamic force drives sediment movement, which induces the bed scour around piles. The severe scour may reduce the stability of the structure, leading to its failure [2]. With respect to this issue, a lot of work has been conducted through experiments [3–5], which mainly focused on the prediction of the maximum scour depth using empirical or semi-empirical equations [6,7]. However, the application of the existing predictive equations to complex flow conditions is problematic or even leads to unreasonable predictions when applying them to real situations [8–10]. The main reason is the lack of a comprehensive understanding of the mechanism of pile group scour, such as the flow fields and hydrodynamics responsible for the occurrence of scour, as well as the sediment dynamics during the scouring process. In reality, the flow field around the pile group changes with the scour development, and the varied flow characteristics within the developing scour holes may also influence the sediment transport near the bed, or even form a sheet flow regime in the case of high bed-shear stress conditions and suspension as the dominating transport modes [11,12]. Therefore, it is necessary to study the evolution of the flow field and its dynamic

characteristics during the process of pile-group scouring, which is also the first step to further study of the resultant sediment dynamic.

The relevant studies on the flow field during the scouring process have been mostly confined to the uniform monopile or single pier. For the earlier studies, Melville and Raudkivi (1977) [13] experimentally studied the flow patterns around a single pier at the initial, middle, and equilibrium scour stages. Graf and Istiarto (2002) [14] utilized an acoustic Doppler velocity profiler to measure the mean velocity components, turbulence intensity, turbulence kinetic energy, and Reynolds stresses in several vertical planes around a circular pier within the equilibrium scour hole. Muzzammil et al. (2003) [15,16] found a horseshoe vortex is generated in front of a monopile, and they further explored the variations of the position, size, and rotation frequency of the horseshoe vortex with the development of scour hole. Dey and Raikar (2007) [17] utilized an acoustic Doppler velocimeter (ADV) to measure the flow field within the developing scour holes when the scour depths are 0.25, 0.5, 0.75, and 1.0 times the maximum equilibrium depth. Similarly, Ashish et al. (2012) [18,19] studied the flow patterns and the turbulence characteristics using an ADV within the developing scour holes around a circular compound pier. Das et al. (2013, 2014) [20,21] used an ADV to measure the flow fields in the scour hole around the piers of different shapes and obtained the relationships of vorticity and circulation of the horseshoe vortex with the scour depth and Reynolds number. The detailed flow field can be acquired via the numerical simulation of computational fluid dynamics (CFD). Kirkil et al. (2008, 2009) [22,23] and Link et al. (2012) [24] utilized the large eddy simulation (LES) and detached eddy simulation (DES) to get the three-dimensional flow fields, particularly the dynamic characteristics of the horseshoe vortex in a scour hole around a circular cylinder. In general, the above-mentioned studies have shown that the flow features around a cylinder are linked with down flow, horseshoe vortex, and wake vortices, and these different components of the flow pattern might play important roles in the process of local scour.

To the best of our knowledge, rather limited studies have focused on the scour process and the associated flow characteristics around the pile group. Compared with the monopile, the flow fields around a pile group are more complicated due to the complexity of pile structures and the interaction of piles. Ataie-Ashtiani and Aslani-Kordkandi (2013) [25] compared the flow patterns around two circular piers in tandem with that around a single pier. They found that the presence of a downstream pier changes the flow structure to a great extent, particularly in the near-wake region, and the pier spacing influences the type of flow regime in the tandem case. Beheshti and Ataie-Ashtiani (2016) [26] measured the flow field around a complex bridge pier (consisting of a pile cap and a 2×4 pile group), and analyzed the mean velocities, turbulence intensities, and Reynolds stresses at different horizontal and vertical planes; however, they mainly focused on the flow field in the upper region of the scour hole and ignored the flow field near the bottom of the scour hole as well as the gap between the piles. Ataie-Ashtiani and Aslani-Kordkandi (2012) [27] presented the flow patterns around two-circular piles positioned in side-by-side arrangement with and without a scour hole, and the flow fields in the gap region (between the two piles) were also investigated. Das and Mazumdar (2015) [28] investigated the characteristics of horseshoe vortex in the equilibrium scour hole around two eccentric circular piles. The aforementioned studies show that the flow fields of multiple-cylinder configurations involve complex interactions between the shear layers, vortices, wakes, and Karman vortex streets [29,30]. However, they only focused on the flow structure in equilibrium scour hole, and for the flow in the intermediate scour hole, the relevant studies are scarce. Local scour at a pile group initiates at, or close to, the side of individual piles, while the scour hole of each pile grows in both depth and volume and then overlaps with each other at the regions of the gaps [31]. Local scour around pile group is time-dependent [32], and the corresponding flow fields as well as its effect on bed scour likewise change over time. Therefore, we emphasize again that it is necessary to study the variations of flow fields and hydrodynamic characteristic with the development of scour holes to deepen our understanding of the scouring process around a pile group.

The main objective of the present study is to explore the evolution of a flow field and hydrodynamic characteristics around a pile group (four piles with 2 × 2 arrangement) with the development of scour hole. The time-averaged and turbulent flow fields in the symmetry plane of the pile group were systematically analyzed. Moreover, the variations of hydrodynamic (including both mean and turbulent) characteristics within the developing scour holes were quantitatively analyzed. Then the spatial distribution of the flow characteristics around the pile group within the scour hole was analyzed. Additionally, the energy spectra analysis of instantaneous velocity was conducted to identify different scales of turbulence eddies in this issue. This paper aims at providing novel insight into the flow field within scour hole around pile group placed in loose sediment, and it is also a first step for further exploring the mechanism of local scour around pile group.

2. Experimental Setup and Methodology

Experiments were performed in a flume (6 m long, 0.25 m wide, and 0.25 m deep) at Beijing Jiaotong University. The flume was filled with quartz sand with specific mass ρ_s = 2650 kg/m^3 and median diameter d_{50} = 0.6 mm. A four-pile group with a 2 × 2 arrangement was mounted vertically in the sand at approximately 4 m from the flume inlet where a fully developed flow was attained [15,26]. Each pile was modeled by a circular cylinder made of clear Perspex tubes with a diameter of D = 1 cm. The face-to-face distance of the piles was set as G = 1.5D. The blockage ratio (i.e., flume width to diameter) in the experiment was 7.14, which is near the lower limit of the acceptable range by referencing previous relevant studies [17]. The experimental setup of this work is depicted in detail in Figure 1.

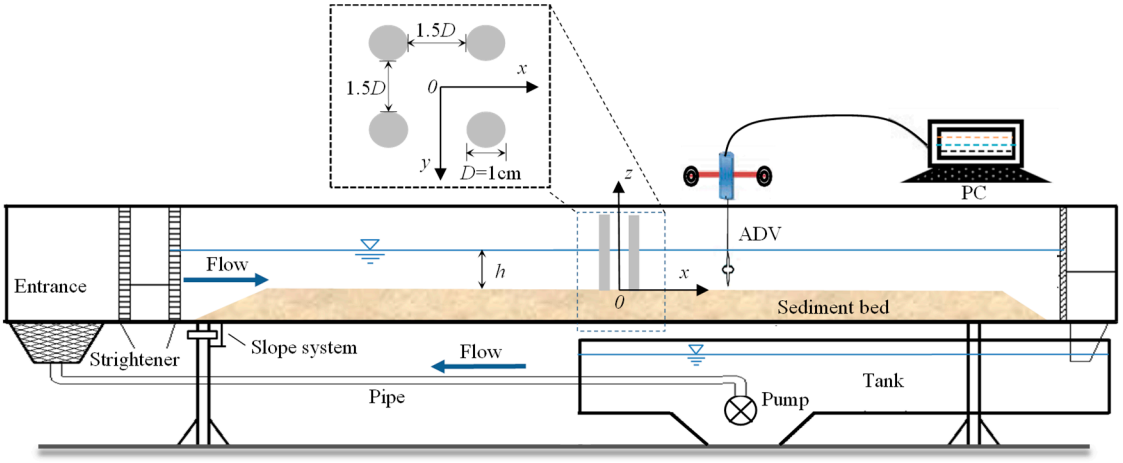

Figure 1. Experimental setup.

The tests were carried out under a uniform incoming flow condition with the inflow discharge of Q = 2.92 × 10^{-3} m^3/s over a bottom slope of J = 0.6‰. The flow depth was kept as h = 5 cm by adjusting the tailgate, and the undisturbed depth-averaged approach flow velocity (measured in the flume centerline at 10D upstream of the pile group) was equal to U_0 = 0.233 m/s.

The undisturbed Shields parameter was calculated as $\Theta_0 = u_*^2/[(\rho_s - \rho)/\rho]gd_{50}$ = 0.029, where u_* (=0.016 m/s) was the bed friction velocity obtained from the best fitting of a log-law profile of the measured velocity at the upstream approach flow, g is the gravitational acceleration, and ρ is the fluid density. According to the Shields curve, the critical Shields parameter to initiate the bed sediment is Θ_{cr} = 0.033. Given that $\Theta_0 < \Theta_{cr}$ (i.e., the far-field bed sediment was not in motion), the tests were conducted in a clear-water scour condition.

The origin of the Cartesian coordinate system was defined as the center of the pile group on its bottom surface, as shown in Figure 1. The instantaneous velocity components were denoted as u for the streamwise, v for the transverse and w for the vertical direction along the x-, y-, and z-axes, respectively.

Such instantaneous flow velocities could be separated into mean (U, V, W) and fluctuating (u', v', w') components according to Reynolds decomposition (i.e., $u = U + u'$). The mean velocity is obtained by averaging the instantaneous velocity, that is:

$$U = \frac{1}{T}\int_0^T u\,\mathrm{d}t\ ,\ V = \frac{1}{T}\int_0^T v\,\mathrm{d}t,\ W = \frac{1}{T}\int_0^T w\,\mathrm{d}t \tag{1}$$

where T is the sampling duration of the instantaneous velocity, that is 120 s in this experiment. The turbulence intensity can be expressed statistically as the standard deviation of the velocity time series. Thus, u_{rms} ($= \sqrt{\overline{u'^2}}$) is the streamwise turbulence intensity, and likewise, v_{rms} ($= \sqrt{\overline{v'^2}}$) and w_{rms} ($= \sqrt{\overline{w'^2}}$) represent the transverse and vertical turbulence intensities, respectively. In addition, the vorticity was calculated using the forward difference technique [33], and normalized by the pile diameter and incoming flow velocity, i.e., $\omega^+ = (\partial U/\partial z - \partial W/\partial x)\ D/U_0$.

Figure 2 shows the development of the scour depth at the upstream pile and downstream pile with time, which demonstrates a high scouring rate for the early stage, and the scouring phenomenon almost reached equilibrium after 240 min. The flow fields at four typical moments around the pile group were measured, including $t/t_e = 0$, $1/120$, $1/20$, and 1, where t_e (=240 min) was the time required to achieving the equilibrium scour in the present experiment. The corresponding maximum scour depth h_s at each time was 0, 2/7, 4/7, and 1 times of the equilibrium scour depth h_e (=2.35 cm in this experiment). The instantaneous three-dimensional velocity components within the scour holes at four moments were captured using a NorTek Acoustic Doppler Velocimeter (ADV) Vectrino II (Rud, Norway), which is equipped with a four-receiver down-looking probe in order to conduct velocity measurements within the scour holes. During the experiment, when the scour time reached a required moment for the flow field measurement, the flow was stopped and the water was drained out. Finally, the bed was frozen by spraying glue uniformly over the scoured bed, and thus the fixed bed facilitated measurements using the ADV.

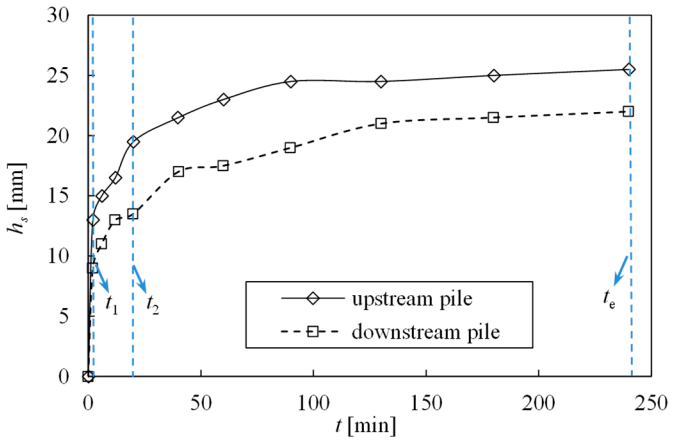

Figure 2. Temporal development of the maximum scour depth.

The scour holes that typically developed were, in fact, reasonably symmetric about the symmetry plane of the pile group, hence describing the flow filed in half-space along the centerline ($y/D \geq 0$ as shown in Figure 2) seems particularly valuable. The measurements were carried out at seven vertical sections (y/D = 0, 0.65, 1.85, 2.5, 3.5, 4.5, 5.5) along the transverse directions of the channel. Among them, the sections of $y/D = 0$ and 0.65 were located in the gap region between the two rows of piles, and the remaining sections were located outside the pile group. In each section, a number of measuring perpendiculars with a spacing of 5 mm along the x-direction were arranged. Taking the horizontal plane $z/D = 0$ in the case of $h_s/h_e = 1$ as an example, the horizontal layout of the vertical lines is shown in Figure 3a. Figure 3b presents the vertical arrangement of the measuring points at the section $y/D = 0$ in the condition of $h_s/h_e = 1$. Since the velocity gradient in the near-bed region

was large and the near-bed flow played an important role on the sediment motion, the measuring points close to the bed surface were refined with the vertical distance of adjacent points of 1 mm. The measurement grid got a little sparser at the upper flow region, up to a spacing of 2 mm and then relaxed to 5 mm. The ADV sampling frequency was set to 200 Hz, and the sampling duration T was set to 120 s, which contained 24,000 samples. This sampling duration was referenced to other relevant experiments [28], and we also made a convergence test to confirm that this duration was sufficient to achieve statistically time-independent quantities. Measurements were filtered using WinADV program (Bureau of Reclamation's Water Resources Research Laboratory) to reject points with a correlation coefficient less than 0.70 and signal to noise ratio less than 15 [34], and the output data from ADV was filtered using the spike removal algorithm of Wahl (2003) [35].

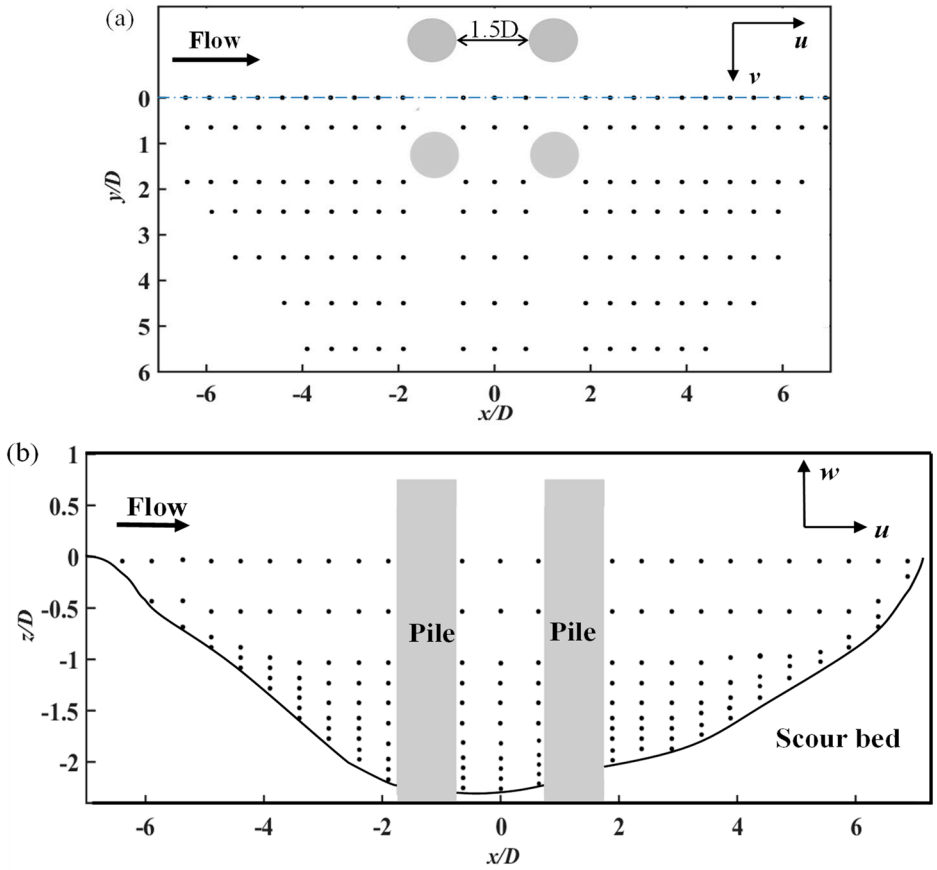

Figure 3. Measurement grid of ADV: (**a**) locations of measurement points in horizontal planes of $z/D = 0$; (**b**) locations of measurement points at vertical section of $y/D = 0$.

The measurement uncertainties mainly included bias errors in the ADV measured velocities and spatial location of these velocities. By time-averaging of a long sampling duration (120 s) with a large number of instantaneous velocity samples (24,000), the uncertainty of the ADV measured mean velocity U was approximate $\pm 0.5\%$ based on our early tests. If the velocity is expressed in a non-dimensional form, uncertainty was introduced through the normalization velocity U_0. The normalization velocity was the far upstream velocity and has been evaluated as the ratio between the flow rate and the water depth. Both the flow rate and water depth were measured with an uncertainty equal to $\pm 0.5\%$. For the present tests at a flow rate of 2.92×10^{-3} m^3/s and a water depth of 5 cm, the normalization velocity U_0 had an uncertainty of $\pm 2.0\%$. The normalized time-averaged velocity had an uncertainty of $\pm 2.6\%$. These estimates were overstated for a high velocity and understated for a low velocity. Assuming the spatial location of the measured points had an uncertainty of $\pm 5\%$, the spatial derivatives $\partial U/\partial z$ were $\pm 5.8\%$. The uncertainty concerning the vorticity doubled because it involved two derivatives.

The uncertainty of the dimensionless vorticity was further increased due to the uncertainty of the normalization velocity. This led to an uncertainty of the normalized vorticity equalling to ±13.9% [36].

In order to guarantee a fully developed approach flow, the velocity distribution in the vertical direction at roughly 0.5 m upstream from the pile group was measured using ADV. Figure 4 shows the profiles of the mean streamwise velocity and turbulent stresses. For the rough-wall surface, the streamwise mean velocity distribution is given by:

$$U/u_* = \frac{1}{\kappa}\ln\left(\frac{u_* z}{\nu}\right) + B - \Delta B \tag{2}$$

where κ (=0.4) is the von Karman constant, B (=5.5) is a constant, and ν is the kinematic viscosity of water. ΔB is the roughness function, which is related to the roughness Reynolds number ${k_s}^+$. Ligrani and Moffat (1986) [37] suggested that the relation between ΔB and ${k_s}^+$ was the following:

$$\Delta B = \left(\frac{1}{\kappa}\ln k_s^+ - 3.3\right) \times \sin\left[0.4258\left(\ln k_s^+ - 0.811\right)\right] \tag{3}$$

where ${k_s}^+$ (=$u_* k_s/\nu$), and the equivalent roughness height k_s is usually set to the median diameter d_{50} of bed material. The bed friction velocity u_* obtained from the best fitting of a log-law profile was equal to 0.016 m/s. The measured velocity data fit the log-law profile theoretically in the turbulent core area (Figure 4a) and the turbulent stresses also fit well with the theoretical result (Figure 4b), which indicates a fully developed approaching flow was maintained.

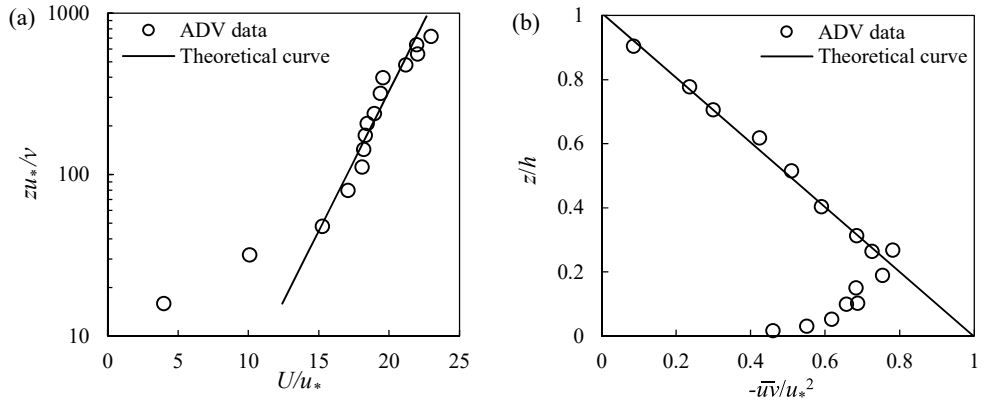

Figure 4. Profiles of (**a**) mean streamwise velocity and (**b**) turbulent stress in the upstream far away from the pile group.

3. Hydrodynamic Characteristics for Developing Scour Holes

3.1. Evolution of Time-Averaged Flow and Characteristics

Figure 5a–c exhibit the mean velocity vectors at the symmetrical plane of the pile group (i.e., $y/D = 0$) for the three case of h_s/h_e = 2/7, 4/7, and 1, in which the magnitude and direction of velocity vectors are $\sqrt{U^2 + W^2}$ and arctan (W/U) respectively. It can be seen that the downward flow combined with reverse flow occurred in the upstream region and give rise to an elliptical vortex structure, which is commonly known as a horseshoe vortex system [38]. This can be attributed to the fact that under the present arrangement of the pile group and flow condition, the general blockage effect of the pile group was strong. Figure 5c demonstrates clearly that the horseshoe vortex was a forced vortex, as the velocity increased in the outward direction from the core of the vortex, which is qualitatively similar to the results of monopile tested by Dey and Raikar (2007) [17]. Comparing the flow field for different cases, the horseshoe vortex became more obvious as the scour hole dimension increased. In the gap region between the tandem piles, the flow direction was inclined downward in the present experiment, which was in contrast to the findings of up-flow feature for a flat-bed case

without a scour hole [25]. Besides, the downward inclination tended to be more significant with the development of the scour hole, indicating that the presence of the scour hole affected the flow field.

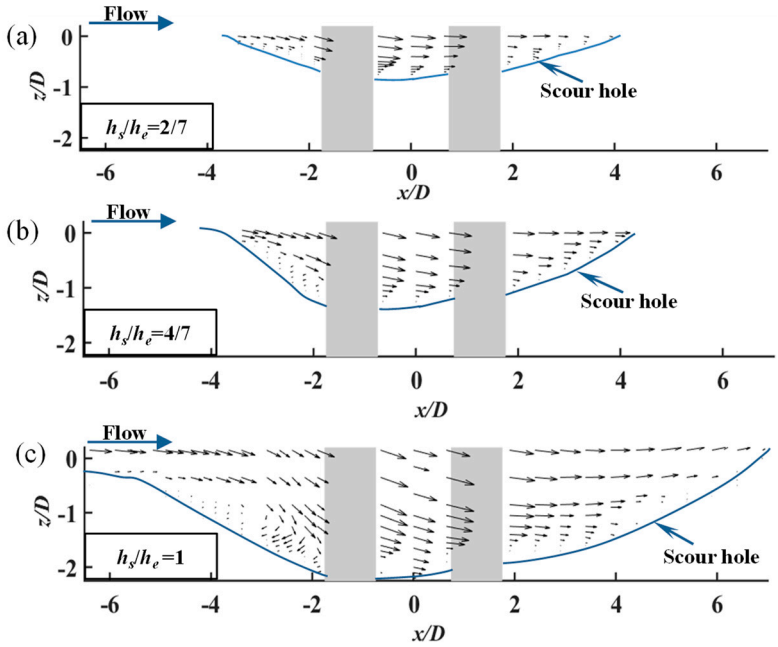

Figure 5. Velocity vectors in the symmetry plane within developing scour holes for (**a**) $h_s/h_e = 2/7$, (**b**) $h_s/h_e = 4/7$, and (**c**) $h_s/h_e = 1$.

Figure 6 compares the contours of the time-averaged vorticity and streamlines at the upstream region of the symmetry plane within developing scour holes. From the distribution of vorticity, it was observed that an elongated patch of high counter-rotating vorticity concentrated in the near-bed region, which was induced by the horseshoe vortex. A similar phenomenon was also found in previous studies [22,39,40]. Moreover, the magnitude of the vorticity generally decreased as the scour depth increased, which meant that the horseshoe vortex induced hydrodynamic force became weak with the development of scour holes.

We defined the location where the streamline bent downward with an inclination more than 10° with the horizontal as the upper periphery of the horseshoe vortex [18], and defined the length of the major axis as D_v, which were approximately equal to 15, 20, and 36 mm for the three scour hole cases. It was noticeable that the lengths of the minor and major axis of the horseshoe vortex increased as the dimension of the scour hole increased. Further up, Figure 7 demonstrates the variation of D_v with the scour depth h_s for the present data, as well as the single circular pile data from the previous study were also included [13,14,17,19]. It was found that the relationship between D_v and h_s conformed to the power law, which can be expressed as follows:

$$D_v = 2.7641 h_s^{\ 0.8187} \ (R^2 = 0.9942) \tag{4}$$

where R^2 is the correlation coefficient.

In general, with the development of scour holes, the size of the horseshoe vortex increases whereas the vorticity induced by the horseshoe vortex decreases and its strength becomes weakened. This is potentially one of the possible reasons leading to the reduction of the scour rate [16].

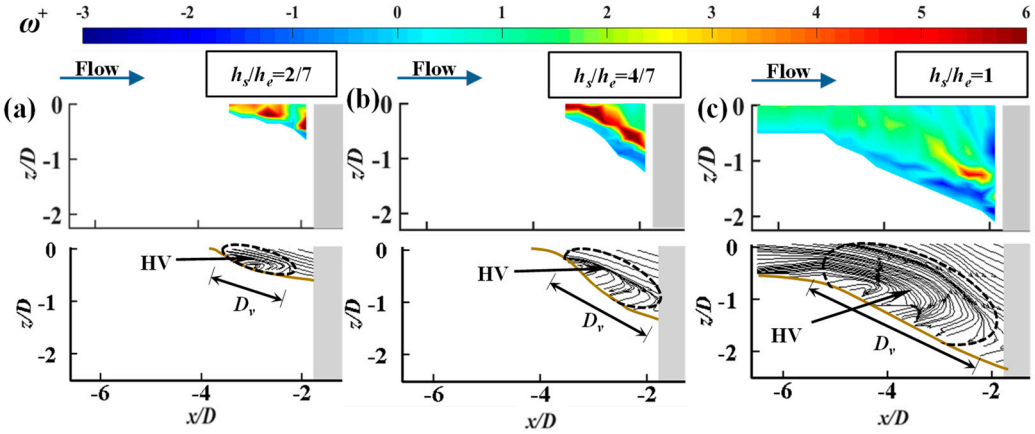

Figure 6. Contours of vorticity ω^+ and streamlines upstream of the symmetry plane within developing scour holes for (**a**) $h_s/h_e = 2/7$, (**b**) $h_s/h_e = 4/7$, and (**c**) $h_s/h_e = 1$.

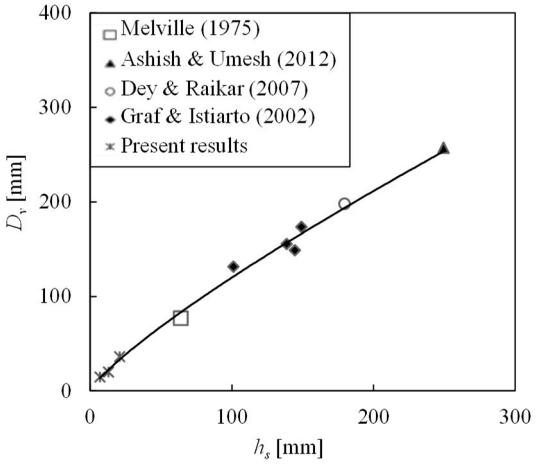

Figure 7. Variation of the major axis of the horseshoe vortex (D_v) with the scour depth (h_s).

Figure 8 depicts the contours of the mean velocity components in the symmetry plane for the three scour hole cases of $h_s/h_e = 2/7$, 4/7, and 1. Only the results of velocity in the x- and z-directions are presented since the transverse velocity in the symmetry plane was small and negligible. The variables in the figure are represented by dimensionless values, i.e., $U^+ = U/U_0$ and $W^+ = W/U_0$. Figure 8a demonstrates that the values of U^+ near the bed in the upstream of the pile group was negative due to the formation of a reverse flow induced by the horseshoe vortex. The area and extreme value of the reverse flow increased with the increase of the scour depth, and the reverse flow was measured with a maximum velocity of almost $0.4U_0$ in the case of $h_s/h_e = 1$. At both the gap and downstream regions of pile group, U^+ was positive in all three scour hole cases and the values were greater than that of upstream of the pile group. For instance, the maximum value of U^+ in the gap could reach up to $1.2U_0$ in the case of $h_s/h_e = 2/7$. This result implies that the flow between the parallel piles was accelerated into the scour hole due to the flow contraction, and the flow maintained its high velocity up to downstream of the pile group [27]. The intense downward flow (e.g., the blue region shown in Figure 8b) was found near the upper region of the upstream pile, and the magnitude of the downward flow increased as the dimensions of scour holes increased. In the wake of the pile group, an upward flow was observed to satisfy the continuity of the flow [27].

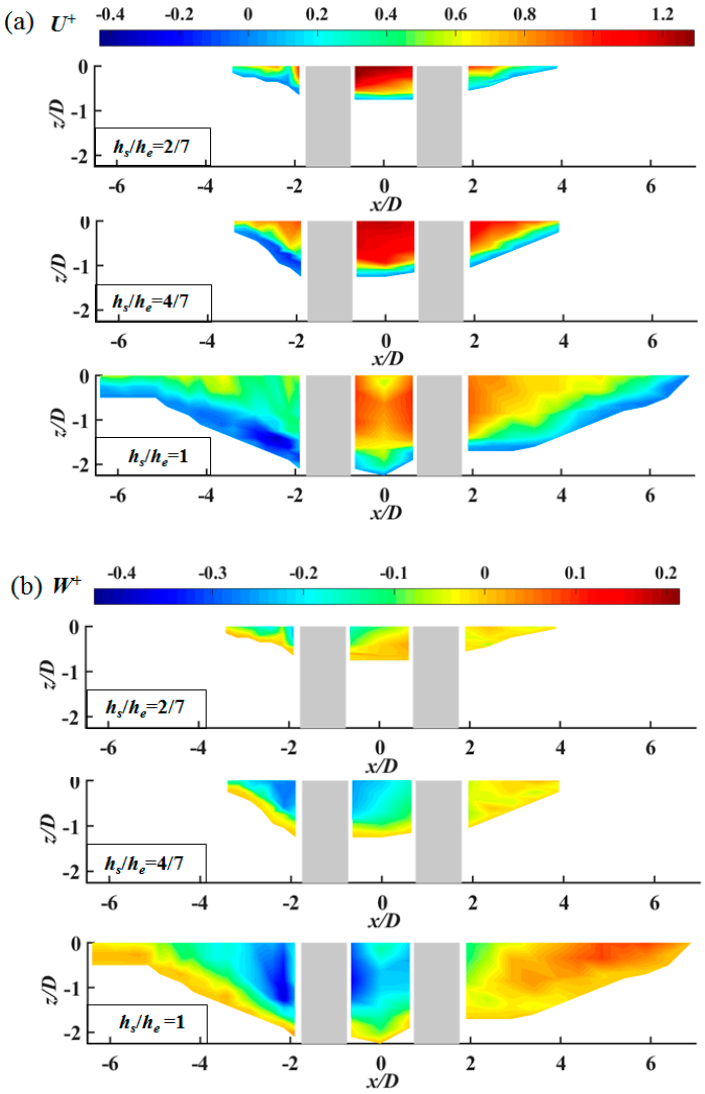

Figure 8. Velocity contours of (**a**) U^+ and (**b**) W^+ in the symmetry plane within developing scour holes.

3.2. Evolution of Time-Averaged Flow and Characteristics

The turbulent characteristics of the flow within the scour hole around the pile group play important roles in the mechanism for sediment transport and the bed scour [41]. Figure 9 demonstrates the contours of the turbulence intensity for different scour holes, in which the non-dimensional values of $u_{rms}{}^+ = u_{rms}/U_0$ and $w_{rms}{}^+ = w_{rms}/U_0$ were used to represent the turbulent intensities in the x- and z-directions, respectively. It clearly shows that the magnitude of $u_{rms}{}^+$ between the two piles was greater than that of the upstream and downstream area. The elevated $w_{rms}{}^+$ zone corresponds to the locations where the downward flow occurs (as shown in Figure 8b). More importantly, the turbulence intensities in the case of $h_s/h_e = 1$ were significantly increased compared to the cases of $h_s/h_e = 2/7$ and $4/7$.

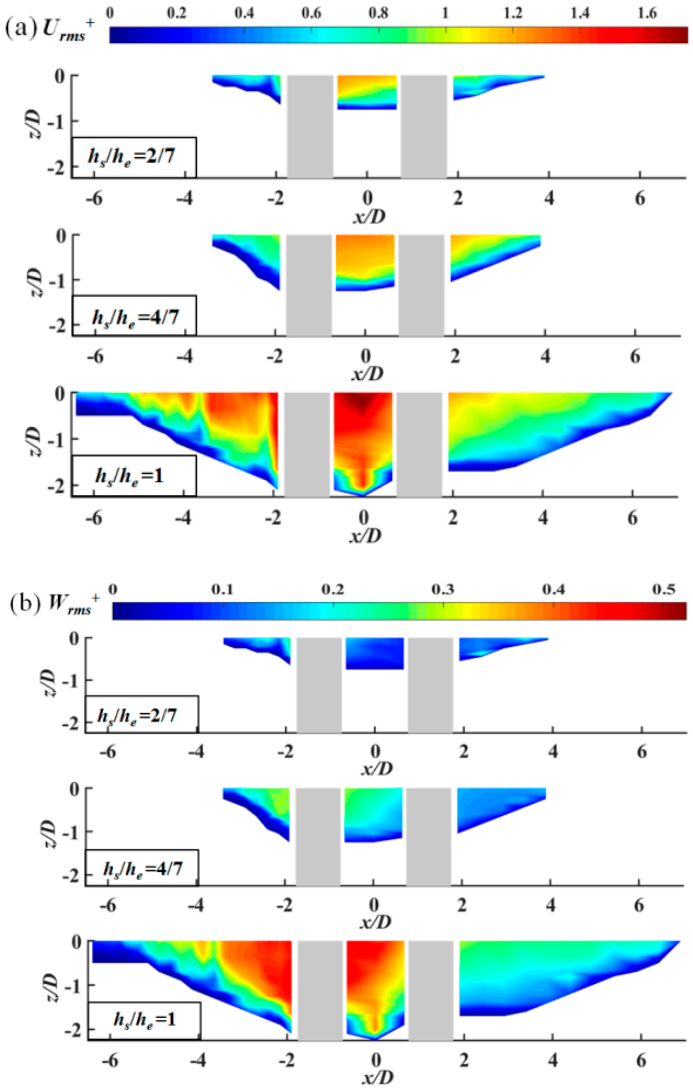

Figure 9. Contours of (**a**) $u_{rms}{}^+$ and (**b**) $w_{rms}{}^+$ in the symmetry plane for developing scour holes.

In order to quantify the variations of the mean velocity and turbulent characteristics with the development of the scour hole, Figure 10 plots a comprehensive comparison of mean velocities and turbulent intensities versus the dimensionless scour depth h_s/h_e, including the extreme values of U^+, W^+ (the symbol "[ ]$_m$" represents the extreme value of the variable), the dimensionless combined velocity $U_T^+ = \sqrt{U^2 + W^2}/U_0$, the extreme values of $u_{rms}{}^+$, $w_{rms}{}^+$ in three regions (i.e., upstream and downstream of pile group, and the gap between tandem piles). The scour rate, r_s, was also included as a subplot. Generally, for the three regions, with the development of the scour hole, the values of r_s, $[U^+]_m$ and $[U_T{}^+]_m$ decreased while the absolute values of $[W^+]_m$, $[w_{rms}{}^+]_m$ and $[u_{rms}{}^+]_m$ increased. Specifically, the magnitude of $[U^+]_m$ for h_s/h_e = 1 in the upstream region was approximate 0.8 times that of h_s/h_e = 2/7. The increased value of $[W^+]_m$ indicates that the down- or up-flow became stronger with the development of the scour hole. The maximum velocities of the downward and upwelling flow in the equilibrium scour hole could reach $0.38U_0$ and $0.12U_0$, respectively. However, the decreasing tendency of the combined velocity $[U_T{}^+]_m$ implies that the mean flow intensity generally decreased with the scour hole development. Meanwhile, the enhanced $[w_{rms}{}^+]_m$ and $[u_{rms}{}^+]_m$ implies that the turbulence became more intense with the development of the scour hole due to the turbulent mixing of the fluid as a result of vortical flow.

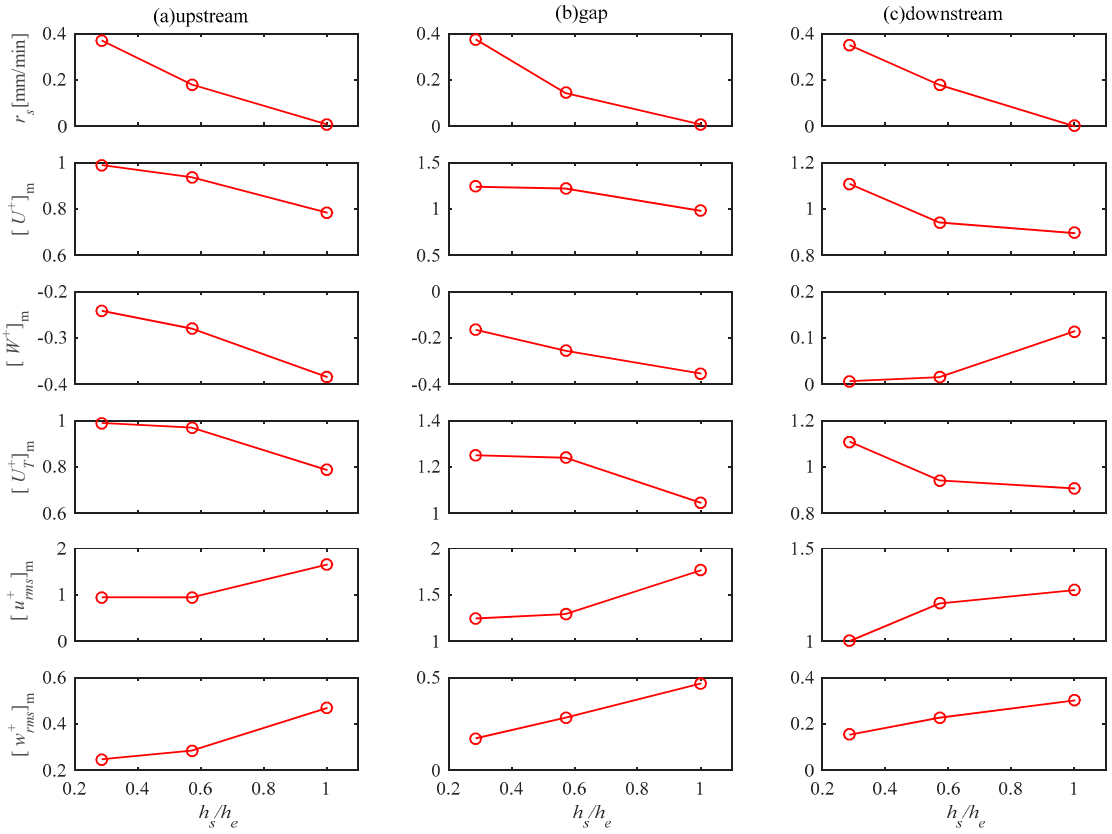

Figure 10. Variation of mean velocities and turbulent intensities with scour depth: (**a**) upstream, (**b**) gap, and (**c**) downstream.

A comprehensive analysis combining the results of turbulence intensity and mean velocity shows that as the scour holes develops, the mean flow around the pile group decreased while the fluctuating component increased simultaneously, which implies that much more mean energy has been transferred to the turbulent energy with the scour hole development. In Figure 11, the time histories of the instantaneous velocity at a measured point (located in the upstream region at the height of Δz = 5 mm above the bed surface) for the cases of h_s/h_e = 2/7 and h_s/h_e = 1 are given. We only exhibit the results for a period of time among the entire sampling duration. Figure 11 clearly shows that the velocity fluctuation under equilibrium scour condition (h_s/h_e = 1) was more prominent, and at the same time, the mean velocity was lower. According to the phenomenon of sediment movement observed in the local scour test [42,43], it is known that, in the late scouring process, although the sediment incipient motion may occur under strong turbulence, the main factor driving sediment transport (i.e., mean flow) was weakened and thus may have caused the decrease of the scour rate.

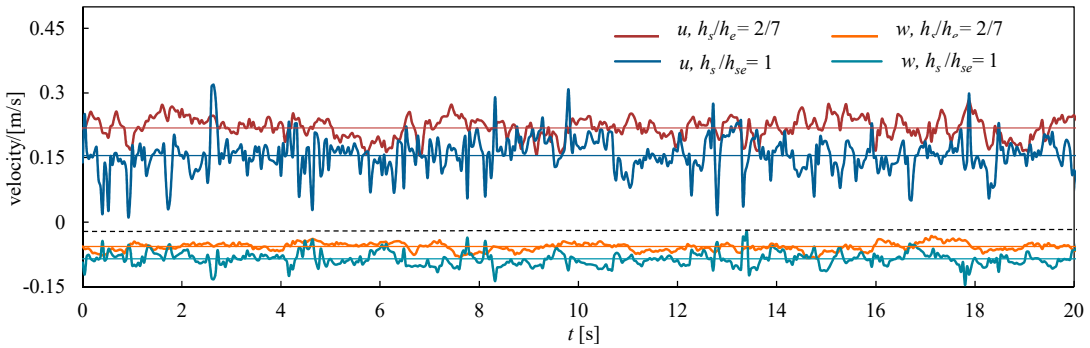

Figure 11. Time histories of instantaneous velocity for intermediate and equilibrium scour holes.

3.3. Bed Shear Velocity with the Scour Hole Development

In this section, the distributions of mean bed shear velocity on the line of symmetry plane for different scour holes are analyzed. The estimates of bed shear velocity are based on the mean streamwise velocities u_1 of the first measurement point at a vertical distance of $z_1 \approx 1$ mm above the bed level, and then normalized with respect to the bed friction velocity u_* of the incoming flow. According to the following Equation (4) [14,18], we can find that the bed shear velocity is closely related to the bed shear stress τ:

$$\tau = \rho(\nu + \nu_T)\frac{u_1}{z_1} \tag{5}$$

where ρ is the water density and ν_T is the eddy viscosity. Therefore, the distribution of the non-dimensional shear velocity $u_n = u_1/u_*$ can also be used to demonstrate the variation tendency of the bed shear stress under the effect of the horseshoe vortex within the changing scour hole.

Figure 12 depicts the variations of bed shear velocity for different scour holes in the upstream and downstream regions of the pile group. In the approach region outside of the scour hole, the magnitude of u_n was large and positive, while u_n in the scoured region was greatly reduced and became negative due to the formation of a horseshoe vortex, as plotted in Figure 12a. In addition, there was a peak value near the pile and the positions of the maximum values of u_n tended to be more upstream with increasing scour depth, e.g., $x/D = -2.41$ for $h_s/h_e = 4/7$ and $x/D = -2.73$ for $h_s/h_e = 1$. For the downstream of the pile group, u_n was entirely positive and a peak value appeared at the far away position ($x/D = 3.7$). By comparing the values of the distributed u_n between the two scour hole cases, it was evident that the magnitudes of u_n for the case of $h_s/h_e = 1$ were generally less than the case of $h_s/h_e = 4/7$, both upstream and downstream of the pile group. This demonstrates that the bed shear velocity was reduced with the development of the scour hole, which further results in the decreased scour rate.

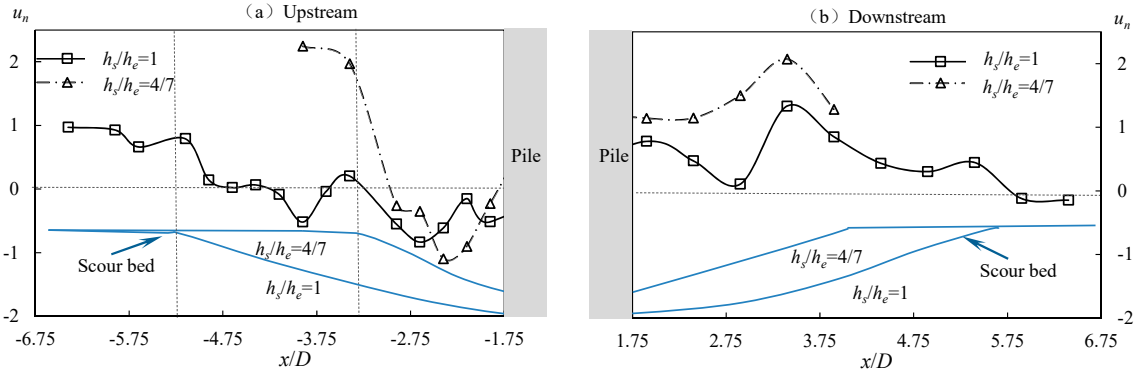

Figure 12. Distributions of bed shear velocity in the symmetry plane for (**a**) upstream and (**b**) downstream of the pile group.

4. Spatial Variation of Flow Characteristics

4.1. Mean Streamline around the Pile Group

Figure 13 exhibits the three-dimensional streamline sketch around the pile group within the equilibrium scour hole, and the contours of the total flow velocity magnitude at different vertical sections in a spanwise direction are also included. The horseshoe vortex (HV) upstream of pile group and the lateral flow around pile group could be observed using the streamlines. The high velocity magnitudes were found in the inner part of pile group as well as downstream of the outer area. The reason may be the effect of flow contraction by the pile group and restriction of the downstream slope of the scour hole, respectively.

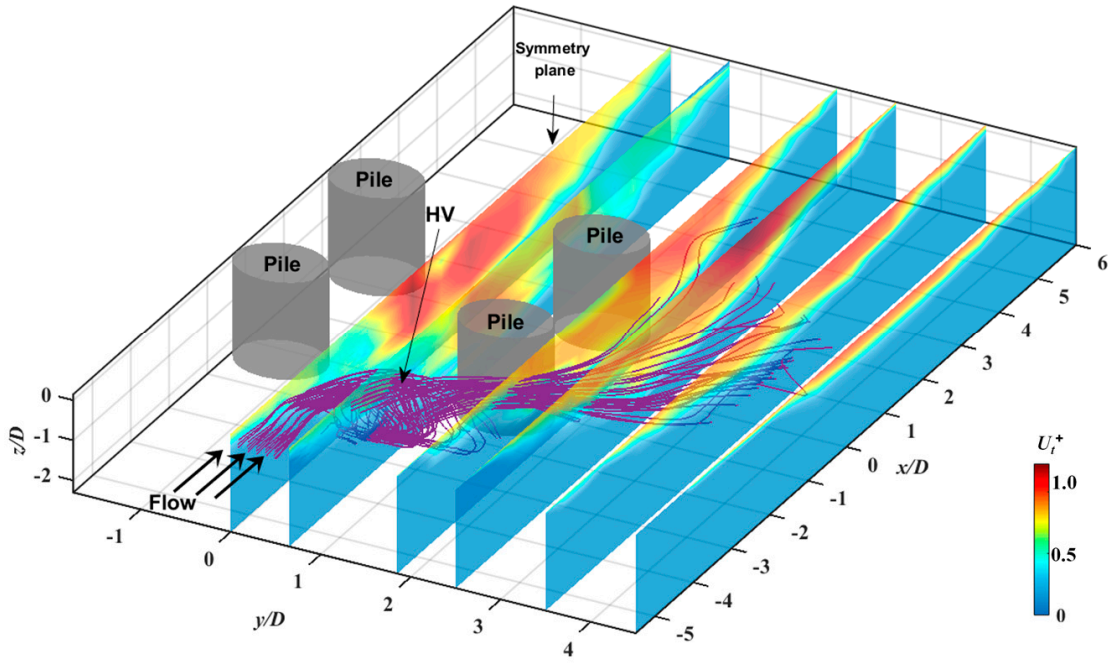

Figure 13. Three-dimensional streamline and contours of the total velocity at different longitudinal sections within the equilibrium scour hole.

We had observed from the experiments of local scouring around the pile group that an independent inverted conical scour hole was formed at the base of each pile for intermediate scour stages (i.e., $h_s/h_e = 2/7$ and $4/7$). Subsequently, the scour hole of each pile gradually merged during the scouring process. Finally, the equilibrium scour hole became a single semi-circular shape [6,44]. In the following analysis, the cases of $h_s/h_e = 4/7$ and 1 were chosen to analyze the spatial distribution of flow characteristics around the pile group. Figure 14 illustrates the trend of two-dimensional streamlines in the horizontal plane of $z/D = 0$ for the two cases. The phenomenon of shear layer reattachment was observed in the gap region between the two tandem piles. According to the classification of the types of wake interference behavior from the literature [30], the local flow pattern in the case of $h_s/h_e = 4/7$ is similar to the "reattachment" regime, whereas the local flow of $h_s/h_e = 1$ is more like an "extended-body" regime (for more description, see Figure 4 of Reference [30]). The reasons are two-fold: (1) for the case of $h_s/h_e = 4/7$, the shear layers from the upstream pile could no longer enclose the downstream pile, but instead reattached onto the downstream pile; (2) for the case of $h_s/h_e = 1$, the separated shear layers from the upstream pile were forced to enclose or wrap around the downstream pile. This situation implies that the four piles behaved more like a whole bluff body when the scour reached equilibrium.

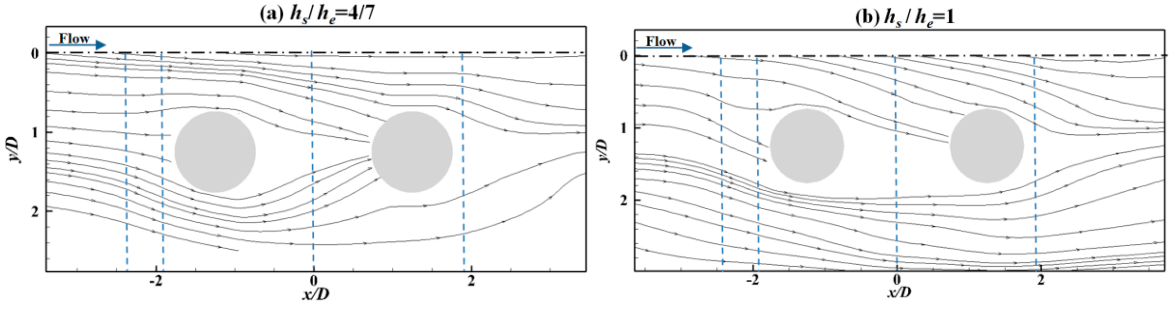

Figure 14. Two-dimensional streamlines at the horizontal planes of $z/D = 0$ for (**a**) $h_s/h_e = 4/7$ and (**b**) $h_s/h_e = 1$.

4.2. Variation of Mean Velocity Profiles

The flow patterns were varied in different positions around the pile group. In order to quantitatively analyze the spatial distribution of flow characteristics, we selected several typical planes (as shown the blue dotted lines in Figure 14), including the sections upstream of the pile group ($x/D = -2.4$ and -1.9), gaps between tandem piles ($x/D = 0$,) and downstream of the pile group ($x/D = 1.9$). The vertical distributions of the non-dimensional mean velocities at different sections were plotted in Figure 15, in which the three components of velocity (U^+, V^+, and W^+) are subplotted in Figure 15a–c, respectively. Here below, we will discuss them separately.

Since the sections of $x/D = -2.4$ and -1.9 were located in the area influenced by the horseshoe vortex upstream of the pile group, the vertical distribution of U^+ in each position appeared as a general trend with the positive value in the upper region and negative value at the near-bed region due to the reverse flow. The values of U^+ at the section of $x/D = 0$ were generally positive along the depth of the flow. Compared with the case of $h_s/h_e = 1$, the velocity increased more rapidly along the flow depth from the bottom of the scoured bed for $h_s/h_e = 4/7$ case and reached a higher maximum value at the position of $z/D = 0$. The distribution of U^+ at the section of $x/D = 1.9$ (i.e., downstream of the pile group) was in good agreement with that of the gaps between the tandem piles; that is, the values along the flow depth were positive at each position and the gradient in the case of $h_s/h_e = 4/7$ was larger than that of $h_s/h_e = 1$.

For the sections of $x/D = -2.4$ and -1.9, the values of V^+ inside the pile group ($y/D = 0$ and 0.65) were significantly smaller than that outside the pile group ($y/D = 1.85$ and 2.5). According to the streamline at the horizontal plane shown in Figure 14, it was found that the flow was directed towards the symmetry plane of the pile group at $x/D = -1.9$ where the local flow induced by the single pile was dominated. However, for the position of $x/D = -2.4$ (more upstream from the pile), the flow was influenced by the interaction of piles, thereby the direction of V^+ deviated from the symmetry plane of the pile group. For the section of $x/D = 0$, V^+ was approximately equal to zero at the position of $y/D = 0$ (i.e., symmetry of the pile group). However, the value of V^+ became large along the transverse direction because the boundary layer separation occurred when the flow went through the upstream pile. For the section of $x/D = 1.9$, the distribution of V^+ inside the pile group was in conformity with that of the $x/D = 0$ section, i.e., the flow was separated by the boundary layer of the downstream pile and the streamlines bent toward the wake of the downstream pile. The values of V^+ outside the pile group was negative, indicating that the flow was directed toward the wake region of downstream pile, which was attributed to the effect of the boundary layer separation of the pile group and the restriction of the scour hole slope.

The magnitude of W^+ was generally negative because of the action of the downward flow, and the value of W^+ was reduced near the bottom of the scour hole. In the case of $h_s/h_e = 1$, the value of W^+ decreased with the increase in y/D, indicating that the downward flow was weakened. For the case of $h_s/h_e = 4/7$, the value of W^+ at the position of $y/D = 0.65$ was larger than that of other locations because the scoured depth of this location was larger and the downward flow became more significant. The distribution of W^+ at the section of $x/D = 1.9$ implies that the downward flow extended downstream of the pile group at the symmetry plane ($y/D = 0$).

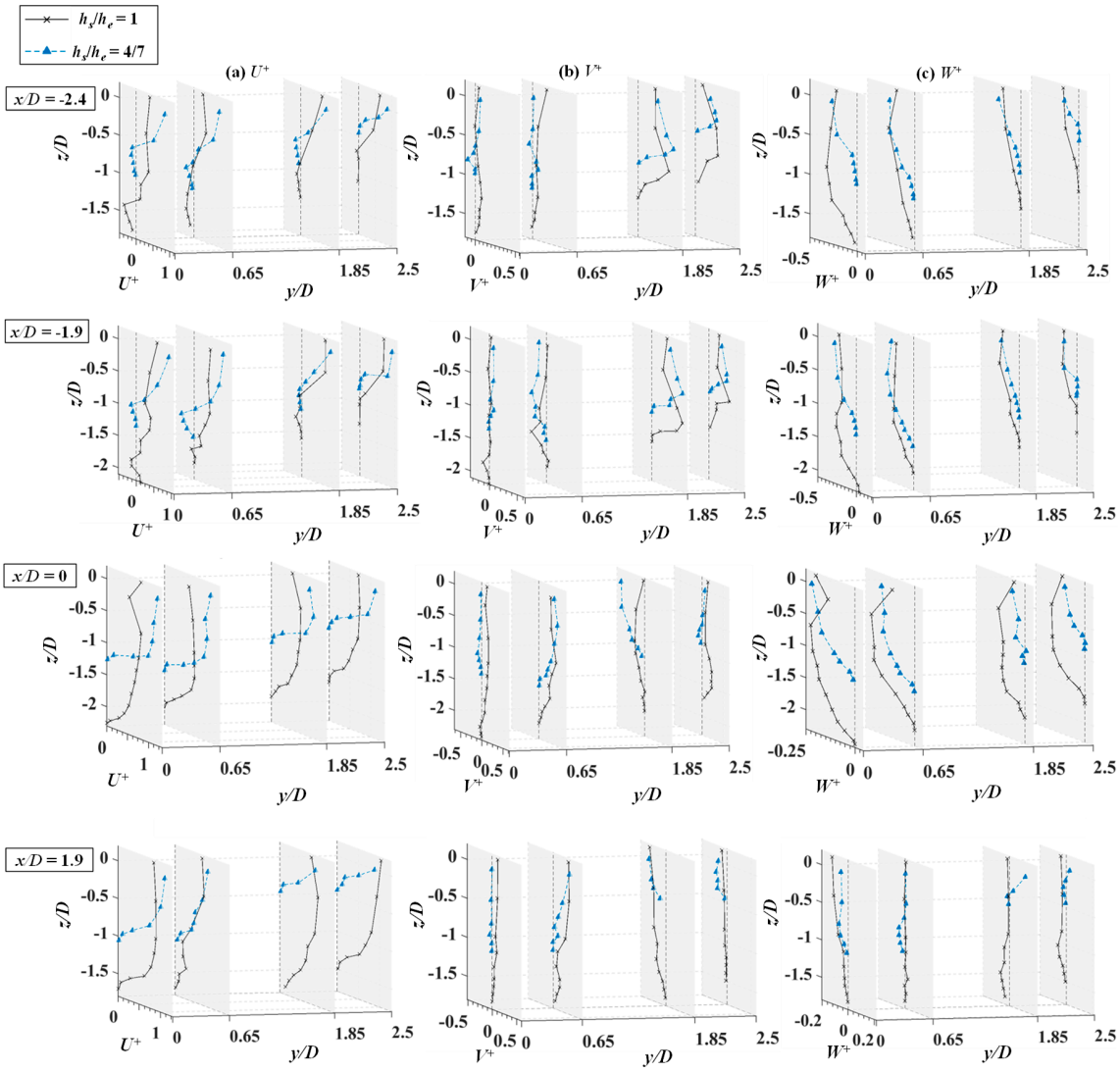

Figure 15. Comparison of the detailed measurements for intermediate and equilibrium scour holes at $x/D = -2.4$ and 1.9: (**a**) U^+; (**b**) V^+; (**c**) W^+.

4.3. Similarity of Turbulence Characteristics

From the above section, it is known that the distribution of mean velocities was distinctive at different positions around the pile group. To further analyze the spatial variation of the turbulence characteristics, the vertical profiles of turbulence intensity components at different scour holes are plotted in Figure 16, including the lines at the upstream of pile group ($x/D = -2.4, -1.9$), gaps between tandem piles ($x/D = 0$), and downstream of the pile group ($x/D = 1.9$). The scales of the variables z, u_{rms}, v_{rms}, and w_{rms} were respectively normalized using $[z]_m$, $[u_{rms}]_m$, $[v_{rms}]_m$ and $[w_{rms}]_m$ for the individual profiles. It is worth noting again that the symbol "$[\ ]_m$" represents the maximum value of the variable. It is shown that all the data at the same position for different scour holes collapsed approximately in a narrow band, which confirmed the similarity of turbulence intensity profiles within the developing scour hole. Additionally, u_{rms}, v_{rms} and w_{rms} increased monotonically along the flow depth from the bottom of the scoured bed and reach the maximum values at $z/D = 0$.

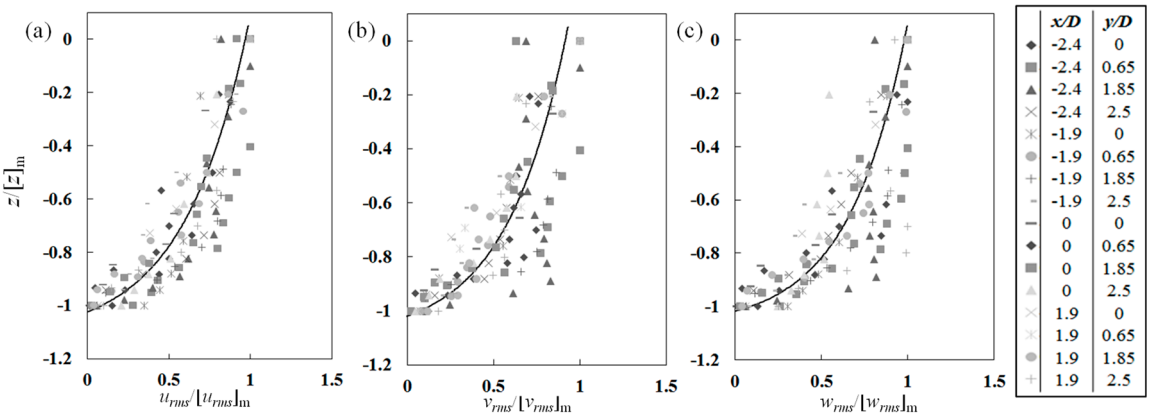

Figure 16. Similarities of the profiles of turbulence intensity components: (**a**) u_{rms}, (**b**) v_{rms}, and (**c**) w_{rms}.

The extreme values of turbulence intensity components (i.e., $[u_{rms}]_m$, $[v_{rms}]_m$, and $[w_{rms}]_m$) for each vertical line at the sections of $x/D = -2.4$, -1.9, 0, and 1.9 along y/D are shown in Figure 17. The values of $[u_{rms}]_m$ and $[v_{rms}]_m$ were significantly larger by about 2–3 orders of magnitude than the values of $[w_{rms}]_m$ in all locations. With the increase of y/D, the disturbance by the piles was weakened, therefore the extreme value of the turbulence intensities decreased.

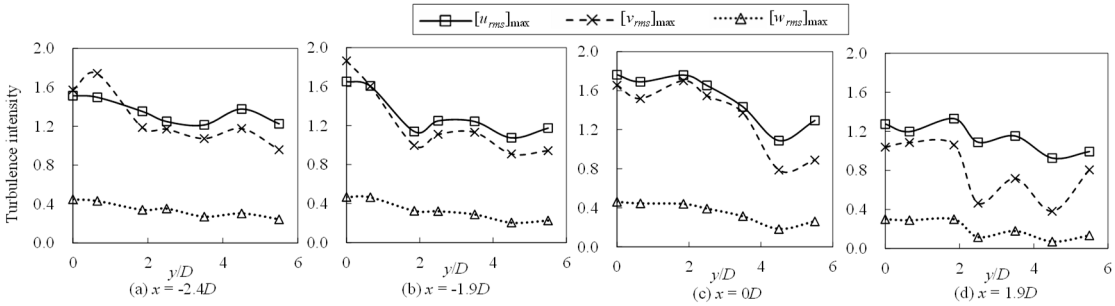

Figure 17. The extreme value of turbulence intensity varies with y/D.

5. Energy Spectra Analysis

For turbulent flows, there exists a continuous and broad range of length or frequency of eddies. During the process of the large-scale eddy (with low frequencies) evolution, a cascade of more and more small-scale eddies appeared. Meanwhile, the turbulent energy was transferred from the large eddies to small eddies, and the small eddies finally diffused and dispersed as a result of viscous dissipation. In order to assess the periodicity and find the dominant vortex-motion frequency of the large-scale coherent structures within the scour holes, energy spectra analysis of the instantaneous velocity was conducted in this section. The power spectrum at the selected points were calculated using fast Fourier transformation (FFT) of the auto-covariance function of velocity time-series data. The presented energy spectra were smoothed using a Tukey lag window and the number of freedom degree of the spectra was two. Figure 18 compares the turbulence energy spectra of velocity components at different regions (i.e., upstream, gap, and downstream of the pile group) for the three scour holes with h_s/h_e = 2/7, 4/7, and 1. The S_u, S_v, and S_w denote the spectral energy density for streamwise, transverse, and vertical velocity components, respectively. For the upstream region, we selected the points near the core of the horseshoe vortex, of which the locations were ($-1.75D$, 0, $-0.6D$), ($-2D$, 0, $-0.8D$), and ($-2.25D$, 0, $-1.4D$) for the three cases of h_s/h_e = 2/7, 4/7, and 1, respectively. For the gap region, the positions of selected points were (0, 0, $-0.5D$) for all three cases. For the downstream region, the points were located at (2.5D, 0, $-0.3D$), (2.5D, 0, $-0.7D$), and (2.5D, 0, $-1D$) for the three scour holes respectively.

The distribution of turbulent energy at different scales shown in Figure 18 indicates that for all the tested cases, the turbulent energy of the entire frequency band was generally enhanced with the increase of scour depth. This result further confirmed that more turbulent energy was extracted from the mean energy as mentioned above in Section 3.2. We also found that the spectrum did not follow the $-5/3$ law, which is valid in the inertial sub-range and exists only if the *Re* is high enough [45]. The $-5/3$ law is based on the equilibrium spectrum hypothesis of the local balance between production and dissipation. However, for the turbulence in the present conditions, the equilibrium hypothesis is not suitable, which can be seen from the deformed spectrum profile in Figure 18. For the band with large frequencies shown in Figure 18a, the spectrum profile of $h_s/h_e = 1$ yielded a steeper slope compared to the cases of $h_s/h_e = 2/7$ and $4/7$. This can be interpreted that more large-scale (low-frequency) eddies or vortex generate and their contribution became dominant, hence the production of turbulence exceeded its dissipation. Moreover, for the larger scales (i.e., lower frequency), noteworthy differences emerged among different scour holes. For the case of $h_s/h_e = 1$, a perceptible peak around a frequency range of $f = 1$ Hz occurred in all three components of the energy spectrum density distribution due to the quasi-periodic oscillation induced by the larger horseshoe vortex. For the cases of $h_s/h_e = 2/7$ and $4/7$, the peaks became less apparent and the corresponding frequency was lower, for the reasons that horseshoe vortex system is not as stable as that in equilibrium scour hole [24].

As shown in Figure 18b, for the same measured point in the gap region of pile group at three different scour holes, the distinction of spectral energy density was generally smaller than that of upstream or downstream points. One can speculate that the turbulence inside the pile group was mainly generated by the disturbance of the four piles and the influence of scour holes change was relatively weak. From the energy spectra of measured points downstream of the pile group shown in Figure 18c, we found that in the case of $h_s/h_e = 2/7$, there was a significant peak region for the larger scales (especially for the distribution of S_u and S_w). This feature resulted from the wake vortex shedding with obvious periodicity. Moreover, the appearance of bimodal phenomena can be observed in the peak region, which may be the evidence of a biased or bistable flow pattern (vortex shedding with two dominant frequencies behind the piles) in agreement with the finding of Sumner et al. [46]. With the development of scour holes, the peak of the energy spectrum became insignificant and eventually disappeared. However, the spectrum energy in the equilibrium $h_s/h_e = 1$ was still larger than that in the non-equilibrium $h_s/h_e = 4/7$ and $2/7$ for the whole frequency range, which may imply that various scale vortices or coherent structures were generated from large-scale roller vortices behind the pile group.

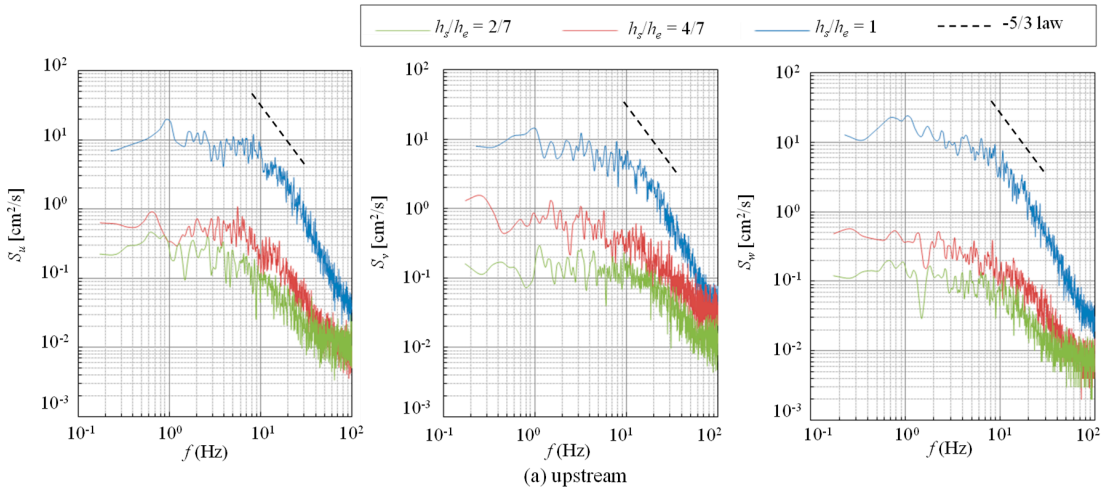

Figure 18. *Cont.*

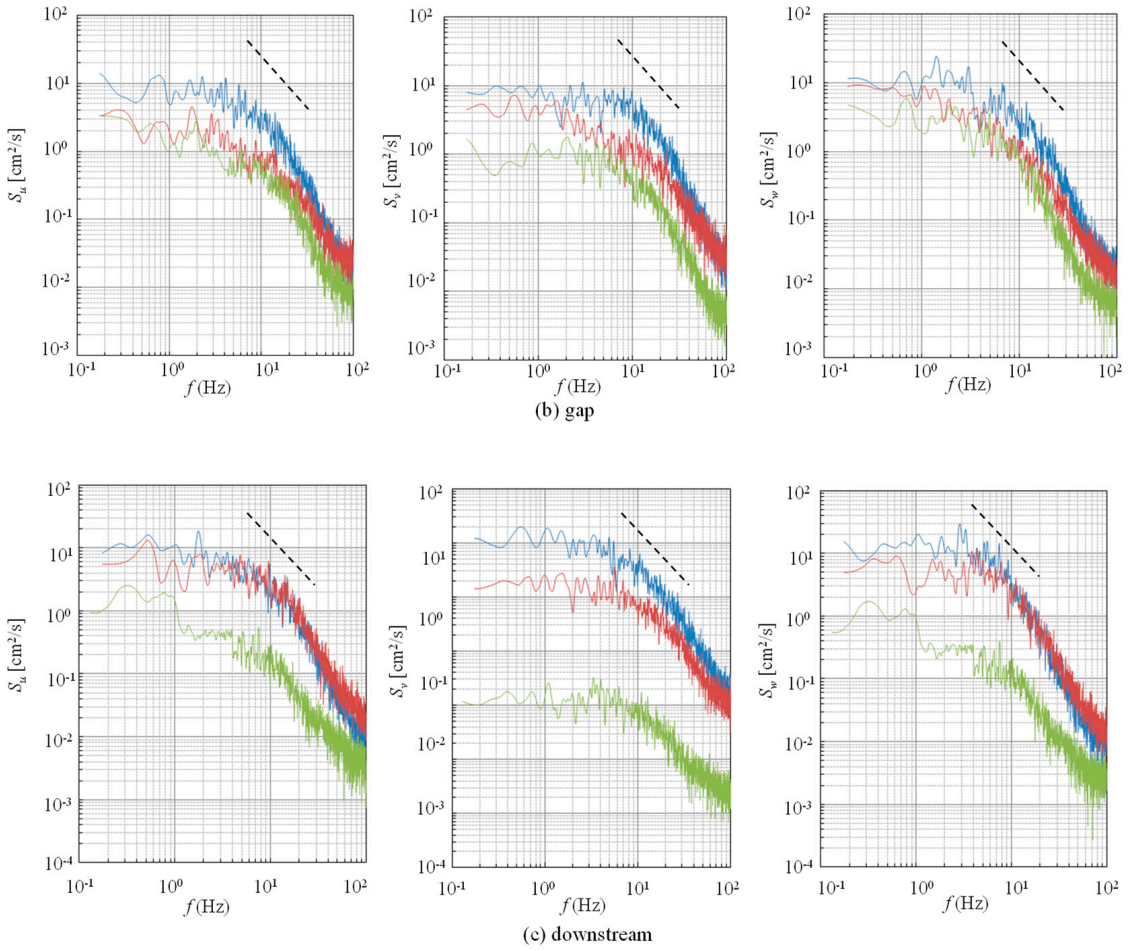

Figure 18. Energy spectral for developing scour holes at the (**a**) upstream, (**b**) gap and (**c**) downstream of the pile group.

6. Conclusions

In this paper, the evolution of hydrodynamic characteristics within the developing scour hole around a pile group was studied by measuring the three-dimensional instantaneous velocities using ADV. The time-averaged flow and turbulence in the symmetry plane and spatial distribution of the flow characteristics at different cross sections were systematically analyzed. Moreover, the variations of hydrodynamic characteristics, including size of horseshoe vortex, vorticity, mean velocity, turbulence intensities, and mean bed shear stresses amplification were quantitatively analyzed with the development of scour holes. Additionally, the energy spectra analysis was conducted with the expectation of identifying different scales of eddies in turbulent flow. The following major conclusions are drawn:

1. Under the present conditions of the pile group arrangement, the reverse flow, downward flow, and horseshoe vortex were observed in the symmetry plane of the upstream region. With the development of scour holes, the size of the horseshoe vortex increased, whereas the vorticity induced by the horseshoe vortex decreased.
2. As the scour depth increased, the mean flow intensity generally decreased, while the turbulence became more intense simultaneously, indicating that much more mean energy was transferred to the turbulent energy in the late scouring process. The main factor driving sediment transport (i.e., mean flow) was weakened and thus may cause the decrease of scour rate.

3. The bed shear velocity within the scour hole was apparently lower compared to that in the approach region outside of the scour hole. A negative peak of the bed shear stress was found near the pile in the upstream region due to the effect of the horseshoe vortex. With the development of the scour hole, the magnitude of the bed shear velocity was generally reduced.
4. An individual horseshoe vortex was formed around each pile in the intermediate scour hole, whereas an integral vortex system was formed in the equilibrium scour hole due to the merging of horseshoe vortexes. The local flow pattern in the gap region between the two tandem piles from reattachment regime turned into an extended-body regime, also implying that the four piles behaved more like a single bluff body as the dimensions of the scour hole increased.
5. The turbulence intensities inside the pile group were relatively large. The vertical distribution of turbulence intensity kept similarity at different locations around the pile group and could collapse in a narrow band.
6. The energy spectra density distribution shows that with the scour hole development, the large-scale horseshoe vortex system was more stable and the dissipation of small-scale eddies were more significant. Meanwhile, the formation and regular shedding of large-scale roller vortices behind the pile group was suppressed due to the expansion of the scour hole.

Author Contributions: Y.Y. conducted the experiments, analyzed the data, and wrote the paper. M.Q. reviewed the paper and provided suggestions for the improvement of the paper. J.L. conducted the analysis of the results and edited the paper; X.M. participated in recording the experimental data.

Acknowledgments: The authors thank the three anonymous reviewers for their constructive comments to improve this paper. This study is financially supported by the National Natural Science Foundation of China [grant number 51578062].

Conflicts of Interest: The authors declare no conflict of interest.

References

1. Rui, L.; Fael, C.; Maia, R. Clear-Water Scour at Pile Groups. *J. Hydraul. Eng.* **2013**, *139*, 1089–1098. [CrossRef]
2. Vittal, N.; Kothyari, U.C.; Haghighat, M. Clear Water Scour around Bridge Pier Group. *J. Hydraul. Eng.* **1994**, *120*, 1309–1318. [CrossRef]
3. Sheppard, D.M.; Melville, B.W.; Demir, H. Evaluation of existing equations for local scour at bridge piers. *J. Hydraul. Eng.* **2013**, *140*, 14–23. [CrossRef]
4. Arneson, L.A.; Zevenbergen, L.W.; Lagasse, P.F. *Evaluating Scour at Bridges*, 5th ed.; Hydraulic Engineering Circular No. 18 (HEC-18); Federal Highway Administration: Washington, DC, USA, 2012; pp. 168–215.
5. Brandimarte, L.; Paron, P.; Baldassarre, G.D. Bridge pier scour: A review of processes, measurements and estimates. *Environ. Eng. Manag. J.* **2012**, *11*, 975–989. [CrossRef]
6. Ataie-Ashtiani, B.; Beheshti, A.A. Experimental Investigation of Clear-Water Local Scour at Pile Groups. *J. Hydraul. Eng.* **2006**, *132*, 1100–1104. [CrossRef]
7. Bayram, A.; Larson, M. Analysis of scour around a group of vertical piles in the field. *J. Waterw. Port Coast. Ocean Eng.* **2000**, *126*, 215–220. [CrossRef]
8. Liang, F.; Wang, C.; Huang, M.; Wang, Y. Experimental observations and evaluations of formulae for local scour at pile groups in steady currents. *Mar. Geotechnol.* **2016**, *35*, 245–255. [CrossRef]
9. Ettema, R.; Constantinescu, G.; Melville, B.W. Flow-field complexity and design estimation of pier-scour depth: Sixty years since Laursen and Toch. *J. Hydraul. Eng.* **2017**, *143*, 03117006. [CrossRef]
10. Qi, M.; Li, J.; Chen, Q. Comparison of existing equations for local scour at bridge piers: Parameter influence and validation. *Nat. Hazards* **2016**, *82*, 2089–2105. [CrossRef]
11. Ribberink, J.S.; Katopodi, I.; Ramadan, K.A.H.; Koelewijn, R.; Longo, S. Sediment transport under (non)-linear waves and currents. In Proceedings of the 24th International Conference on Coastal Engineering, Kobe, Japan, 15–20 June 1994; pp. 2527–2541. [CrossRef]
12. Longo, S. Two-Phase Flow Modeling of Sediment Motion in Sheet-Flows above Plane Beds. *J. Hydraul. Eng.* **2005**, *131*, 366–379. [CrossRef]
13. Melville, B.W.; Raudkivi, A.J. Flow characteristics in local scour at bridge piers. *J. Hydraul. Res.* **1977**, *15*, 373–380. [CrossRef]

14. Graf, W.H.; Istiarto, I. Flow pattern in the scour hole around a cylinder. *J. Hydraul. Res.* **2002**, *40*, 13–20. [CrossRef]
15. Muzzammil, M.; Gangadhariah, T. The mean characteristics of horseshoe vortex at a cylindrical pier. *J. Hydraul. Res.* **2003**, *41*, 285–297. [CrossRef]
16. Muzzammil, M.; Gangadharaiah, T.; Gupta, A.K. An experimental investigation of a horseshoe vortex induced by a bridge pier. *Water Manag.* **2004**, *157*, 109–119. [CrossRef]
17. Dey, S.; Raikar, R.V. Characteristics of horseshoe vortex in developing scour holes at piers. *J. Hydraul. Eng.* **2007**, *133*, 399–413. [CrossRef]
18. Kumar, A.; Kothyari, U.C. Three-Dimensional Flow Characteristics within the Scour Hole around Circular Uniform and Compound Piers. *J. Hydraul. Eng.* **2012**, *138*, 420–429. [CrossRef]
19. Kumar, A.; Kothyari, U.C.; Raju, K.G.R. Flow structure and scour around circular compound bridge piers—A review. *J. Hydro-Environ. Res.* **2012**, *6*, 251–265. [CrossRef]
20. Das, S.; Das, R.; Mazumdar, A. Circulation characteristics of horseshoe vortex in scour region around circular piers. *Water Sci. Eng.* **2013**, *6*, 59–77. [CrossRef]
21. Das, S.; Das, R.; Mazumdar, A. Vorticity and Circulation of Horseshoe Vortex in Equilibrium Scour Holes at Different Piers. *J. Inst. Eng.* **2014**, *95*, 109–115. [CrossRef]
22. Kirkil, G.; Constantinescu, G.; Ettema, R. Detached eddy simulation investigation of turbulence at a circular pier with scour hole. *J. Hydraul. Eng.* **2009**, *135*, 888–901. [CrossRef]
23. Kirkil, G.; Constantinescu, S.G.; Ettema, R. Coherent Structures in the Flow Field around a Circular Cylinder with Scour Hole. *J. Hydraul. Eng.* **2008**, *134*, 82–84. [CrossRef]
24. Link, O.; González, C.; Maldonado, M.; Escauriaza, C. Coherent structure dynamics and sediment particle motion around a cylindrical pier in developing scour holes. *Acta Geophys.* **2012**, *60*, 1689–1719. [CrossRef]
25. Ataie-Ashtiani, B.; Aslani-Kordkandi, A. Flow Field Around Single and Tandem Piers. *Flow Turbul. Combust.* **2013**, *90*, 471–490. [CrossRef]
26. Beheshti, A.A.; Ataie-Ashtiani, B. Scour Hole Influence on Turbulent Flow Field around Complex Bridge Piers. *Flow Turbul. Combust.* **2016**, *97*, 1–24. [CrossRef]
27. Ataie-Ashtiani, B.; Aslani-Kordkandi, A. Flow field around side-by-side piers with and without a scour hole. *Eur. J. Mech.* **2012**, *36*, 152–166. [CrossRef]
28. Das, S.; Mazumdar, A. Turbulence flow field around two eccentric circular piers in scour hole. *Int. J. River Basin Manag.* **2015**, *13*, 343–361. [CrossRef]
29. Zdravkovich, M.M. The effects of interference between circular cylinders in cross flow. *J. Fluids Struct.* **1987**, *1*, 239–261. [CrossRef]
30. Sumner, D. Two circular cylinders in cross-flow: A review. *J. Fluids Struct.* **2010**, *26*, 849–899. [CrossRef]
31. Kim, H.S.; Nabi, M.; Kimura, I. Computational modeling of flow and morphodynamics through rigid-emergent vegetation. *Adv. Water Resour.* **2015**, *84*, 64–86. [CrossRef]
32. Wang, D.; Shao, S.; Li, S.; Shi, Y.; Arikawa, T.; Zhang, H. 3D ISPH erosion model for flow passing a vertical cylinder. *J. Fluids Struct.* **2018**, *78*, 374–399. [CrossRef]
33. Graf, W.H.; Yulistiyanto, B. Experiments on flow around a cylinder; the velocity and vorticity fields. *J. Hydraul. Res.* **1998**, *36*, 637–654. [CrossRef]
34. Kitsikoudis, V.; Kirca, V.S.O.; Yagci, O.; Celik, M.F. Clear-water scour and flow field alteration around an inclined pile. *Coast. Eng.* **2017**, *129*, 59–73. [CrossRef]
35. Wahl, T.L. Discussion of "Despiking Acoustic Doppler Velocimeter Data" by Derek G. Goring and Vladimir I. Nikora. *J. Hydraul. Eng.* **2003**, *129*, 484–487. [CrossRef]
36. Longo, S.; Chiapponi, L.; Clavero, M. Experimental analysis of the coherent structures and turbulence past a hydrofoil in stalling condition beneath a water–air interface. *Eur. J. Mech. B Fluids* **2014**, *43*, 172–182. [CrossRef]
37. Ligrani, P.M.; Moffat, R.J. Structure of transitionally rough and fully rough turbulent boundary layers. *J. Fluid Mech.* **1986**, *162*, 69–98. [CrossRef]
38. Baker, C.J. The laminar horseshoe vortex. *J. Fluid Mech.* **1979**, *95*, 347–367. [CrossRef]
39. Escauriaza, C.; Sotiropoulos, F. Reynolds number effects on the coherent dynamics of the turbulent horseshoe vortex system. *Flow Turbul. Combust.* **2011**, *86*, 231–262. [CrossRef]
40. Kirkil, G.; Constantinescu, G.; Ettema, R. The Horseshoe Vortex System Around a Circular Bridge Pier on Equilibrium Scoured Bed. *Am. Soc. Civ. Eng.* **2005**, 1–12. [CrossRef]

41. Debnath, K.; Manik, M.K.; Mazumder, B.S. Turbulence statistics of flow over scoured cohesive sediment bed around circular cylinder. *Adv. Water Resour.* **2012**, *41*, 18–28. [CrossRef]
42. Amini, A.; Melville, B.W.; Ali, T.M.; Ghazali, A.H. Clear-Water Local Scour around Pile Groups in Shallow-Water Flow. *J. Hydraul. Eng.* **2012**, *138*, 177–185. [CrossRef]
43. Wang, H.; Tang, H.; Liu, Q.; Wang, Y. Local Scouring around Twin Bridge Piers in Open-Channel Flows. *J. Hydraul. Eng.* **2016**, *142*, 06016008. [CrossRef]
44. Kim, H.S.; Nabi, M.; Kimura, I.; Shimizu, Y. Numerical investigation of local scour at two adjacent cylinders. *Adv. Water Resour.* **2014**, *70*, 131–147. [CrossRef]
45. Petti, M.; Longo, S. Turbulence experiments in the swash zone. *Coast. Eng.* **2001**, *43*, 1–24. [CrossRef]
46. Sumner, D.; Wong, S.S.T.; Price, S.J.; Paidoussis, M.P. Fluid behavior of side-by-side circular cylinders in steady cross-flow. *J. Fluids Struct.* **1999**, *13*, 309–338. [CrossRef]